Determining the Sources of Regional Haze in the Southeastern United States Using the CMAQ Model

M. TALAT ODMAN, YONGTAO HU, ALPER UNAL,* AND ARMISTEAD G. RUSSELL

School of Civil and Environmental Engineering, Georgia Institute of Technology, Atlanta, Georgia

JAMES W. BOYLAN

Georgia Department of Natural Resources Environmental Protection Division, Atlanta, Georgia

(Manuscript received 15 February 2006, in final form 2 October 2006)

ABSTRACT

A detailed sensitivity analysis was conducted to help to quantify the impacts of various emission control options in terms of potential visibility improvements at class I national parks and wilderness areas in the southeastern United States. Particulate matter (PM) levels were estimated using the Community Multiscale Air Quality (CMAQ) model, and light extinctions were calculated using the modeled PM concentrations. First, likely changes in visibility at class I areas were estimated for 2018. Then, using emission projections for 2018 as a starting point, the sensitivity of light extinction was evaluated by reducing emissions from various source categories by 30%. Source categories to be analyzed were determined using a tiered approach: any category that showed significant impact in one tier was broken into subcategories for further analysis in the next tier. In the first tier, sulfur dioxide (SO_2), nitrogen oxides, ammonia, volatile organic compound, and primary carbon emissions were reduced uniformly over the entire domain. During summer, when most class I areas experience their worst visibility, reduction of SO_2 emissions was the most effective control strategy. In the second tier, SO_2 sources were separated as ground level and elevated. The elevated sources in 10 southeastern states were differentiated from those in the rest of the domain and broken into three subcategories: coal-fired power plant (CPP), other power plant, and other than power plant [i.e., non–electric generating unit (non EGU)]. The SO_2 emissions from the CPP subcategory had the largest impact on visibility at class I areas, followed by the non-EGU subcategory. In the third tier, emissions from these two subcategories were further broken down by state. Most class I areas were affected by the emissions from several states, indicating the regional nature of the haze problem. Here, the visibility responses to all of the aforementioned emission reductions are quantified and deviations from general trends are identified.

1. Introduction

Fine particulate matter (often referred to as $PM_{2.5}$ to denote particle sizes smaller than 2.5 μm) is a mixture of suspended solid particles and liquid droplets and can impact both human health and the environment. In addition to being seen as a reason for numerous health problems such as asthma, $PM_{2.5}$ is also a major cause of visibility impairment. $PM_{2.5}$ originates from many sources such as fossil fuel combustion, sea salt, windblown dust, and fugitive dust (e.g., road dust, construction, grinding, and agriculture), and it is formed in the atmosphere through chemical transformation of precursor gases. It can travel long distances and affect very large geographic areas. In certain parts of the United States the visual range has been reduced considerably from natural conditions.

Visibility is a measure of the clearness of the atmosphere. Regional haze is the impairment of visibility caused by the presence of PM in the atmosphere and is usually expressed in term of light extinction or haze index. It has been determined that particles of different size and chemical composition can affect visibility very differently (Interagency Monitoring of Protected Vi-

* Current affiliation: MACTEC Federal Programs, Inc., Trenton, New Jersey.

Corresponding author address: M. T. Odman, Georgia Institute of Technology, 311 Ferst Dr., Atlanta, GA 30332-0512.
E-mail: odman@gatech.edu

DOI: 10.1175/2007JAMC1430.1

sual Environments 2000). In particular, $PM_{2.5}$ can scatter and absorb light very efficiently. The contributions of fine sulfate and nitrate particles to haze can be substantial especially in the presence of water vapor. Elemental and organic carbon is also important in visibility degradation while most other particles are viewed as being relatively less important.

The objective of the regional haze rule from the Environmental Protection Agency (EPA 1999) is to achieve natural visibility conditions (no man-made impairment) at national parks and wilderness areas known as class I areas (EPA 2002) by 2064. The rule requires that reasonable progress should be made toward reducing visibility impairment on the 20% worst visibility days. In addition, the rule requires no worsening of visibility on the 20% best visibility days. Every 10 years, progress toward these goals must be demonstrated. The first regional haze state implementation plans (due by December 2007) must demonstrate progress toward natural conditions by evaluating the change in visibility between current conditions (2000–04) and the first progress check point (2014–18). Progress can be measured by comparing the projected visibility on the 20% worst days to a straight line drawn between current visibility (2000–04) and natural conditions (2064) on a haze index versus time graph. However, achieving such a uniform rate of progress at every check point is neither a requirement nor a standard for demonstrating reasonable progress.

Visibility Improvement State and Tribal Association of the Southeast (VISTAS) is the regional planning organization set up by EPA to initiate and coordinate activities associated with the management of regional haze in 10 southeastern states: Alabama (AL), Florida (FL), Georgia (GA), Mississippi (MS), Kentucky (KY), North Carolina (NC), South Carolina (SC), Tennessee (TN), Virginia (VA), and West Virginia (WV). VISTAS is conducting a modeling study with the goal of lowering PM levels and improving visibility in the southeastern United States. This paper reports a detailed sensitivity analysis conducted as part of that study to quantify the contributions of various emission sources to regional haze. The sensitivities are calculated by taking the difference between two air quality model simulations: one with base case and another with reduced emission inputs. This method is known as the "brute force" method (Hwang et al. 1997). The model used here to simulate the air quality is the Community Multiscale Air Quality (CMAQ) model (Byun and Ching 1999).

Brute-force sensitivity analysis has been widely used to aid the design of control strategies for ozone. For example, recently, Marr and Harley (2002) studied the impact of motor vehicle emissions on ozone levels in central California using the California Institute of Technology (CIT) air shed model (Harley et al. 1993). Stein and Lamb (2002), using CMAQ, modeled regional ozone sensitivities over northeastern America. Chang et al. (2002) used the Comprehensive Air Quality Model with Extensions (CAMx; ENVIRON 2006) to estimate the sensitivity of ozone to chlorine emissions in Houston, Texas. Schmidt and Martin (2003) used "CHIMERE," a chemistry-transport model designed for the simulation of photo-oxidant concentrations within the atmospheric boundary layer (Vautard et al. 2001), to calculate ozone sensitivities in Paris, France. Later, Pison and Menut (2004) used the same model, to assess the impact of aircraft emissions on ozone in Paris. Jiang and Fast (2004) used the Pacific Northwest National Laboratory Eulerian Gas and Aerosol Scalable Unified System to model ozone sensitivities to nitrogen oxides (NO_x) and volatile organic compound (VOC) emissions in Houston. Fast and Heilman (2005) used the same model to calculate ozone sensitivities in the Great Lakes region. Oanh and Zhang (2004) studied ozone sensitivities in Thailand with the aid of the Urban Airshed Model (System Applications International, Inc., 1999). Lin et al. (2005) conducted an ozone sensitivity analysis in Texas using CMAQ. Distinct from these studies, Pai et al. (2000) used the brute-force method to calculate the sensitivities of PM, as well as ozone, in central California using the SARMAP Air Quality Model (SARMAP denotes the San Joaquin Valley Air Quality Study/Atmospheric Utility Signatures, Predictions, and Experiments Regional Model Adaptation Project).

A number of other sensitivity analysis methods have been tested and applied in 3D air quality models (AQMs). Automatic differentiation in FORTRAN has found limited use in AQMs (Hwang et al. 1997; Carmichael et al. 1997). Recently, the adjoint method was tried in 3D models such as CHIMERE and Polair3D to conduct ozone sensitivity analyses in Europe (Menut et al. 2000; Mallet and Sportisse 2005). The decoupled direct method (DDM), which provides a very efficient way of calculating several sensitivities in a single model run, became very popular after its implementation in the CIT model (Yang et al. 1997). Odman et al. (2004) used DDM in the Urban to Regional Multiscale model (Boylan et al. 2002) to study the sensitivity of ozone and PM levels to sulfur dioxide (SO_2), NO_x, ammonia (NH_3), and VOC emissions in the southeastern United States. Cohan et al. (2005) implemented DDM in CMAQ to study ozone sensitivities to various source

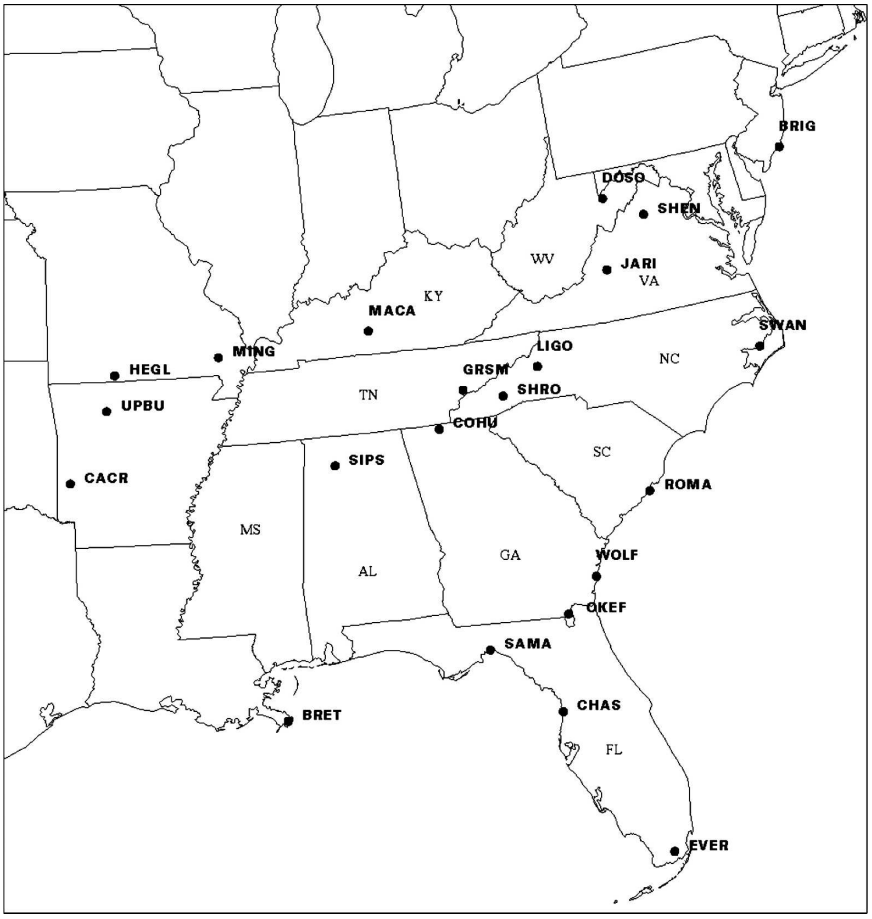

FIG. 1. Modeling domain, 10 VISTAS states, and locations of class I areas.

categories. At the time this project had started, the implementation of DDM for PM sensitivities in the CMAQ model was under way. Later, the implementation was completed (Napelenok et al. 2006) but not in time to be used here.

2. Method

The aerosol module of CMAQ is designed to estimate size resolved and speciated PM concentrations (Binkowski and Roselle 2003). The PM size distribution is represented by the superposition of three lognormal modes: the nucleation and accumulation modes for $PM_{2.5}$ and a coarse mode. $PM_{2.5}$ consists of sulfate, nitrate, ammonium, elemental carbon (EC), organic carbon (OC), and soil components; the coarse mode includes sea salt and dust. The aerosol dynamical processes considered in CMAQ include primary emissions, new particle formation by nucleation, particle growth, coagulation, evaporation/condensation, dry deposition, and scavenging by clouds. Chemical reactions form secondary PM such as sulfate, nitrate, ammonium, and organic compounds. CMAQ is continuously updated to improve the accuracy of its $PM_{2.5}$ predictions (Bhave et al. 2004); the particular version used here was version 4.3.

a. Simulation of $PM_{2.5}$ levels

To model the seasonal variation of PM concentrations, a summer (12–28 July 2001) and a winter (1–21 January 2002) episode were simulated with CMAQ. Inputs to CMAQ were generated using the fifth-generation Pennsylvania State University–National Center for Atmospheric Research Mesoscale Model for meteorology (Grell et al. 1994) and the Sparse Matrix Operator Kernel Emissions model for emissions (Center for Environmental Modeling for Policy Development 2004). Details of the meteorological and emissions modeling can be found elsewhere (Olerud and Sims 2003; Morris et al. 2004).

The horizontal resolution of the CMAQ grid was 12 km over the domain shown in Fig. 1. Nineteen un-

equally spaced vertical layers with finer resolution near the surface extended to a height of approximately 14 km. The lowest four layers were 36 m thick. Earlier evaluations of the effects of the number of layers and layer thicknesses showed that this setup is adequate for modeling surface layer concentrations and deposition fluxes even during stable nighttime conditions (Morris et al. 2004).

Anthropogenic emissions were considered in ground-level and elevated source categories. Ground-level sources include on-road and nonroad mobile sources, area sources, and area fires. Elevated sources include electric generating units (EGUs), other point sources, and point fires. All man-made emissions were projected out to 2018 using growth and control factors; the Integrated Planning Model was used to predict emission rates and controls at all EGUs. Two scenarios were developed to reflect VISTAS's assumptions about future growth and the implementation of regulations and incentives: "on the books" (OTB) and "on the way" (OTW). The main difference between these scenarios is that 2018-OTW includes the clean air interstate rule.

It was assumed that any potential feedback of future land use and emissions on the meteorology would be negligible. Therefore meteorological inputs developed for the July 2001 and January 2002 periods were also used for the 2018 simulations. Biogenic emissions were also assumed to remain constant in the future. Initial and boundary conditions were derived from a 36-km resolution simulation of 2018 over North America. A two-day ramp-up period was used before each episode to dampen the effect of initial conditions.

Using emission projections for 2018 as the base case, emission-reduction simulations were performed and the differences from the base case were recorded. In each simulation, emissions from a particular source category were reduced by 30% from its base-case value and responses of PM concentrations and light extinctions to these reductions were calculated. A tiered approach was used to identify the most important emission species and emission source categories that could be controlled to achieve maximum visibility benefits. This approach first identified the importance of individual emission species (tier 1). Then, the impact of the most important emission source categories were examined for important emission species (tier 2). Finally, the most important emission source categories were further broken down into geographic regions (tier 3). Overall, more than 100 model simulations were conducted. Responses were calculated and visualized for the entire domain but quantitative analysis focused on responses at class I areas.

b. *Sensitivity analysis of visibility to emission reductions*

Light extinction B_{ext} (Mm^{-1}) was calculated as a linear combination of specific pollutant concentrations ($\mu g\ m^{-3}$), component-specific light scattering/absorption coefficients ($m^2\ g^{-1}$), and a dimensionless relative humidity adjustment factor $f(RH)$ using the following equation (Interagency Monitoring of Protected Visual Environments 2000):

$$B_{ext} = 3 \times f(RH) \times ([SO_4^{2-}] + [NO_3^-] + [NH_4^+]) + 4 \times [OC] + 10 \times [EC] + 1 \times [soil] + 0.6 \times [CM] + B_{Rayleigh}. \quad (1)$$

Here, $[SO_4^{2-}]$, $[NO_3^-]$, $[NH_4^+]$, [OC], [EC], and [soil] are the concentrations of $PM_{2.5}$ associated with sulfate, nitrate, ammonium, organic carbon, elemental carbon, and soils, respectively; [CM] is the concentration of coarse PM; and $B_{Rayleigh}$ is the Rayleigh scattering (10 Mm^{-1}). Note that $[NH_4^+]$ is set equal to $0.375 \times [SO_4^{2-}] + 0.29 \times [SO_4^{2-}]$ in Eq. (1) assuming ammonium completely neutralizes sulfate and nitrate to form $SO_4(NH_4)_2$ and NO_3NH_4 (Boylan et al. 2006). Site-specific monthly values based on climatology were used for $f(RH)$. The haze index (HI) is typically expressed in units of deciviews and can be calculated directly from the total light extinction (B_{ext}) by the following equation:

$$HI = 10 \times \ln(B_{ext}/B_{Rayleigh}), \quad (2)$$

where HI is zero for an unpolluted atmosphere and each deciview increase in HI approximates a perceptible decrease in visibility.

The Interagency Monitoring of Protected Visual Environments (IMPROVE) network routinely monitors the composition of $PM_{2.5}$ at the class I areas of the region shown in Fig. 1. The sites are categorized as mountain, coastal, or non-VISTAS in Table 1. The measurements of daily average concentrations are available at each site every third day; therefore, visibility can be calculated only on about ⅓ of the simulated days. Also, because the regional haze rule is concerned only with the 20% best and 20% worst visibility days, only those days were considered in the analysis leaving very few days. There are 1–5 simulated days that represent the 20% best/worst visibility days at each site considered here (Table 1). Classification and Regression Tree (CART) analysis was used to group the meteorological conditions that lead to good/bad visibility at each class I area and to determine the representativeness of simulated days (Douglas et al. 2006). Each day was assigned a weight that characterizes the fre-

TABLE 1. Class I areas in the modeling domain, their categorization as coastal (C), mountain (M), or non-VISTAS (N), and their number of the simulated 20% best and 20% worst visibility days. The number of the worst visibility days during summer is shown in parentheses.

	Site	State	Abbreviation	Class	No. of days	
					Best	Worst (summer)
1	Sipsey	AL	SIPS	M	2	3 (3)
2	Chassahowitzka	FL	CHAS	C	4	2 (1)
3	Everglades	FL	EVER	C	6	1 (0)
4	St. Marks	FL	SAMA	C	4	2 (2)
5	Cohutta	GA	COHU	M	1	2 (2)
6	Okefenokee	GA	OKEF	C	5	4 (3)
7	Wolf Island*	GA	WOLF	C	—	—
8	Mammoth Cave	KY	MACA	M	3	4 (4)
9	Linville Gorge	NC	LIGO	M	4	2 (2)
10	Shining Rock	NC	SHRO	M	4	2 (2)
11	Swanquarter	NC	SWAN	C	5	3 (2)
12	Cape Romain	SC	ROMA	C	5	2 (1)
13	Great Smoky Mountains	TN	GRSM	M	4	2 (2)
14	James River Face	VA	JARI	M	5	1 (1)
15	Shenandoah	VA	SHEN	M	3	3 (3)
16	Dolly Sods	WV	DOSO	M	5	3 (3)
17	Caney Creek	AR	CACR	N	4	5 (5)
18	Upper Buffalo	AR	UPBU	N	3	5 (5)
19	Breton	LA	BRET	N	3	2 (2)
20	Hercules Glades	MO	HEGL	N	2	5 (4)
21	Mingo	MO	MING	N	1	2 (1)
22	Brigantine	NJ	BRIG	N	4	2 (1)

* No visibility data are available at Wolf Island.

quency of occurrence of its meteorological conditions among the 20% best or 20% worst visibility days. Note that the weights are site specific and their sum over the simulated days is unity. Hereinafter, when used in connection with a metric (e.g., light extinction), "20% best or 20% worst visibility" refers to an approximation to that metric obtained by taking the inner product of the CART weights with the values on simulated days.

The modeled concentrations were used in a relative rather than absolute fashion to account for under- and overpredictions by the model. This was done by scaling the modeled future response (i.e., difference in concentrations between the base and reduced emissions cases) $\Delta C_{\text{future}}^{\text{modeled}}$ by the ratio of currently observed concentrations $C_{\text{current}}^{\text{observed}}$ to the modeled current concentrations $C_{\text{current}}^{\text{modeled}}$:

$$\Delta C_{\text{future}} = \frac{C_{\text{current}}^{\text{observed}}}{C_{\text{current}}^{\text{modeled}}} \Delta C_{\text{future}}^{\text{modeled}}. \quad (3)$$

Note that this scaling was applied to each $PM_{2.5}$ species separately. As an example, let us assume that the observed nitrate concentration is zero but the model predicts a nonzero nitrate concentration and a future reduction. In this case, because there is no observed nitrate to be reduced, Eq. (3) will set the response to zero. The scaling was not used in some rare cases when small modeled concentrations unrealistically amplified the response.

The results presented here are only valid for 30% reduction of the specified emission category from the specified region. If one wants to estimate the response to a smaller reduction by scaling the results, it should be realized that an error is introduced because of the nonlinearity of atmospheric response. Prior work has shown that this error would be small for the responses of ozone and $PM_{2.5}$ to domainwide emission reductions (Odman et al. 2002; Hakami et al. 2003; Hakami et al. 2004); however, this might not be true for subdomain reductions. Extrapolation beyond 30% is highly discouraged. In addition, extreme caution should be used in superposing the sensitivities to emissions from different geographic regions or sensitivities to emissions from different source categories. Such deductions can be used during the development of control strategies to give an estimated magnitude and some directional sense as to where to look for emission reductions. However, they should not be used as a substitute for simu-

TABLE 2. Domainwide daily average emissions (Mg) for typical baseline and 2018-OTB and 2018-OTW* scenarios.

	SO_2	NO_x	NH_3	PC	Anthropogenic VOC	Biogenic VOC
Typical baseline (2000–04)						
Jan	30 800	35 400	4770	2820	38 400	9500
Jul	30 100	36 200	4850	2770	37 700	113 500
2018-OTB						
Jan	23 300	22 000	5750	2920	30 600	9500
Jul	21 700	21 200	5850	2870	30 800	113 500
2018-OTW						
Jan	16 100	18 600	5750	2790	30 600	9500
Jul	15 600	20 000	5850	2760	30 800	113 500

* The 2018-OTW scenario assumes the implementation of the CAIR in addition to all the assumptions of 2018-OTB.

lations that demonstrate the effectiveness of a given emission control strategy.

3. Results and discussion

The July 2001 and January 2002 episodes were simulated by Morris et al. (2004) using "actual" emissions. Model estimates for gaseous precursors, ozone, and PM were evaluated using observations from various monitoring networks, including IMPROVE. Among the $PM_{2.5}$ components, sulfate agrees the best with observations: its bias is within ±20% both in summer and in winter. Nitrate concentrations are overestimated by 50%–100% in winter and organic carbon is underestimated by 80%–100% in summer (Morris et al. 2005; Tesche et al. 2006). Here, the final modeling setup recommended by Morris et al. (2004) was used in all simulations.

A second set of simulations of the same episodes were conducted using the "typical" baseline emissions. The difference in these emissions from the actual case is that the EGU and fire emissions were averaged over a longer time period (e.g., 3 yr for EGUs) to remove anomalies and make them more representative of the 2000–04 baseline period. The results of these typical baseline simulations were used as $C_{\text{current}}^{\text{modeled}}$ in Eq. (3) above for scaling modeled responses.

a. Visibility simulated for 2018

Domainwide SO_2, NO_x, NH_3, VOC, and primary carbon (PC) emissions under the 2018-OTB and OTW scenarios are compared with their typical baseline (2000–04) levels in Table 2. Under the OTB scenario, the largest relative reductions are in NO_x emissions (38% in January and 43% in July). The second largest relative reduction is in SO_2 emissions (24% in January and 28% in July) followed by anthropogenic VOC emissions (20% in January and 18% in July). The PC emissions increase by 4% in this case. The spatial distribution of these emission changes is highly nonuniform: the magnitude as well as the direction of the change varies from one place to another. In general, NO_x emissions are reduced, most notably along the Ohio River valley, but not everywhere. SO_2 emissions are also reduced in the same region, with some exceptions, but increases are dominant in some southeastern states and along the Gulf of Mexico coast.

The 2018-OTW scenario includes further reductions due to the implementation of the clean air interstate rule (CAIR). In comparison with the OTB scenario, reductions of SO_2 emissions almost double (48% reduction both in January and July when compared with their typical baseline values). Winter and summer NO_x emissions are, respectively, 47% and 45% less than their typical baseline values. No further controls are applied to anthropogenic VOC emissions. The PC emissions are assumed to remain near their baseline values. Without further change under the OTW scenario ammonia emissions increase by 21% in all cases and biogenic VOC emissions are assumed to remain constant.

Typical baseline (2000–04) values of total light extinction B_{ext} range from 30 to 260 Mm^{-1} at the class I areas of the modeling domain (Fig. 2a). Figure 2b shows the expected changes in light extinction ΔB_{ext} on the 20% best and 20% worst visibility days under the OTB and OTW scenarios in 2018. Negative ΔB_{ext}, plotted upward from the origin indicates an improvement in visibility while positive ΔB_{ext} signals visibility degradation. The range and the average of the values of ΔB_{ext} are shown for each one of the three categories of class I areas: coastal, mountain, and non-VISTAS. Under the OTB scenario, ΔB_{ext} on the 20% best visibility days range from +2.76 to −9.00 with an average of -0.83 Mm^{-1} at coastal sites. Visibility is expected to degrade at Cape Romain, the Everglades, and

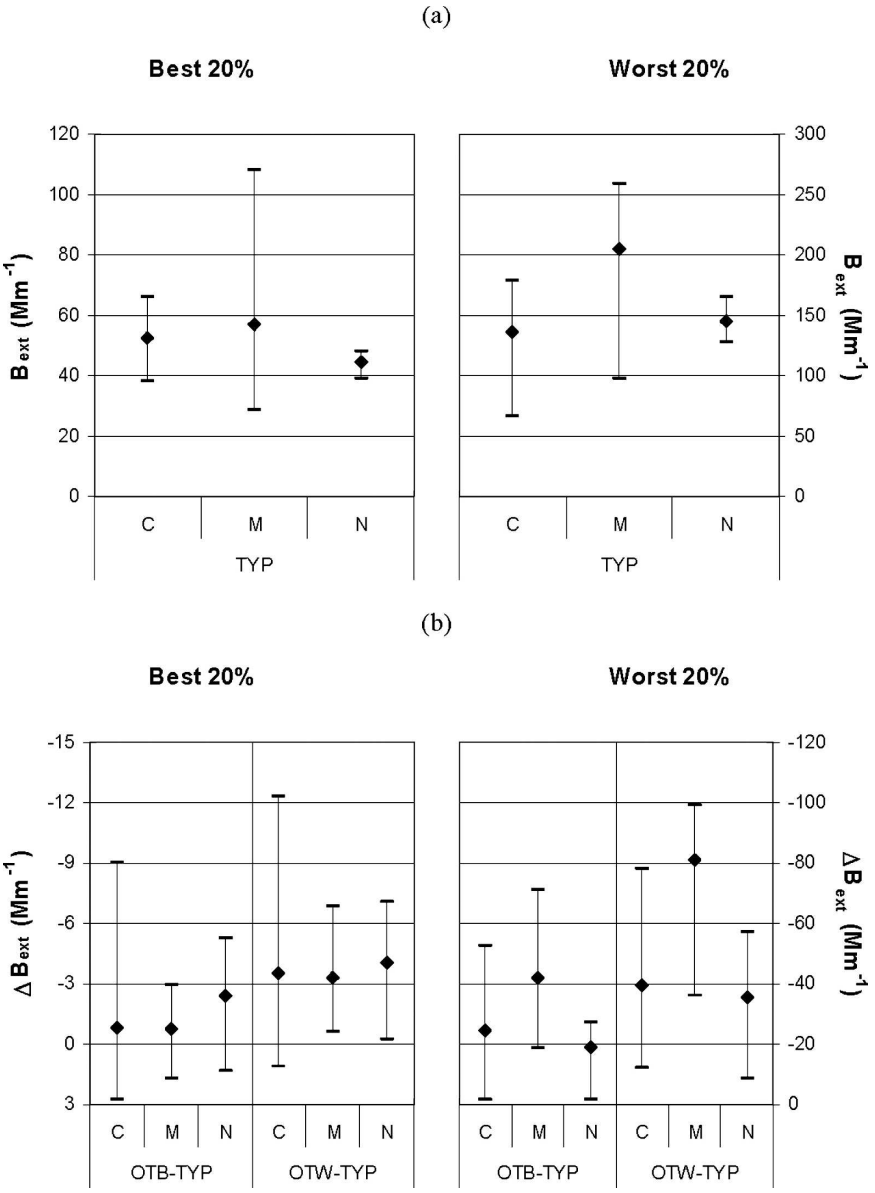

FIG. 2. (a) Typical baseline (TYP) values of light extinction and (b) its expected changes under the 2018-OTB and 2018-OTW scenarios on the 20% best and 20% worst visibility days at coastal (C), mountain (M), and non-VISTAS (N) class I areas. Diamonds denote the average for each category while bars mark the range.

Okefenokee as a result of increases in the levels of nitrate, EC, OC, and coarse matter. Note that most of the best visibility days occur during summer at these sites. SO_2 controls and increasing ammonia emissions (Table 2) can result in increased nitrate levels as a result of more ammonia becoming available to react with nitric acid and form nitrate aerosols (Odman et al. 2004). At these sites, the increases in nitrate levels are larger than the decreases in sulfate levels resulting in a net increase of $PM_{2.5}$ and degradation of visibility.

At mountain sites, where the best visibility days generally occur in winter, ΔB_{ext} range from +1.71 to −2.92 with an average of $-0.72\ Mm^{-1}$. Visibility degradations are expected at the Great Smoky Mountains and, to a smaller extent, at Linville Gorge and Dolly Sods because of local increases in sulfate levels on the 20% best visibility days. Among the non-VISTAS sites ΔB_{ext} range from +1.37 to −5.25 with an average of $-2.37\ Mm^{-1}$; visibility is expected to degrade at Breton and Mingo.

Under the more stringent controls of the OTW scenario, no mountain or non-VISTAS site is expected to experience visibility degradation in 2018. The difference that CAIR makes is sufficient to put almost all of the sites in compliance with the regional haze rule (i.e., no visibility degradation on the 20% best visibility days); therefore, there is no need for additional controls on the best visibility days except at Cape Romain and the Everglades. Average B_{ext} decreases rise to 3.53, 3.26, and 4.03 Mm^{-1} for the coastal, mountain, and non-VISTAS categories, respectively.

On the 20% worst visibility days, visibility in 2018 improves at all sites under both OTB and OTW scenarios. Note that the scale for these days is shown on the right side of Fig. 2b. Worst visibility days generally occur during summer except at some coastal sites, which may experience their poorest visibility in winter. Under the OTB scenario, ΔB_{ext} ranges from -1.63 to -52.7 with an average of -24.3 Mm^{-1} at coastal sites, from -18.5 to -70.8 with an average of -41.9 Mm^{-1} at mountain sites, and from -1.72 to -26.8 with an average of -18.9 Mm^{-1} at non-VISTAS sites. These improvements are largely because of decreases in sulfate and ammonium levels as a result of SO_2 emission reductions. The largest improvements in visibility are expected at mountain sites. The decreases in sulfate levels are generally larger in southern (e.g., Cohutta and Great Smoky Mountains) than western (e.g., Mammoth Cave) and northern (e.g., Dolly Sods) class I areas of the VISTAS region. Some mountain (e.g., Great Smoky Mountains) and coastal (e.g., Okefenokee) sites in the South will experience increases in nitrate levels and some coastal (e.g., Chassahowitzka) and non-VISTAS sites (e.g., Upper Buffalo) will experience increases in OC levels, but these increases are not sufficient to counter the benefits of SO_2 reductions. Shenandoah experiences the largest decrease in nitrate levels among all sites.

Under the OTW scenario, all sites experience greater improvements in visibility on the 20% worst days. Average ΔB_{ext} rise to -39.7, -81.2, and -35.6 Mm^{-1} at the coastal, mountain, and non-VISTAS sites, respectively. Responses to further emission reductions will be analyzed next.

b. Sensitivity of visibility to emission reductions

The 2018-OTB emissions were taken as the base case for the sensitivity analysis. CAIR was promulgated after the analysis had started. Given that 2018-OTW scenario might be more realistic, the first tier described below was repeated with 2018-OTW emissions as the base case. However, because the sensitivities for both scenarios were very similar, the decision was made to continue the analysis, which was well under way, using the 2018-OTB emissions.

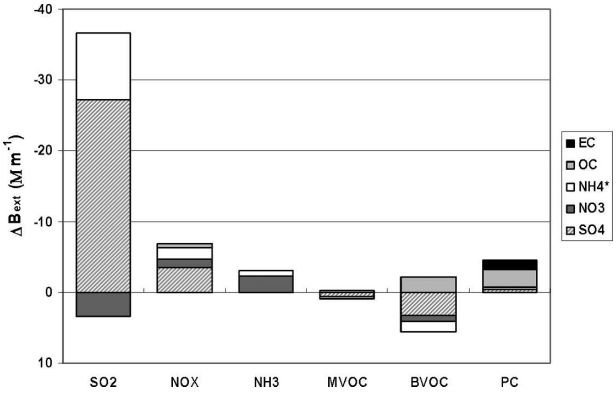

FIG. 3. Contributions of sulfate, nitrate, ammonium (where the asterisk indicates the assumption that all ammonium is in the form of ammonium sulfate and ammonium nitrate), OC, and EC in the response of light extinction to a 30% domainwide reduction of SO_2, NO_x, NH_3, anthropogenic (M)VOC, biogenic (B)VOC, and PC emissions on the 20% worst visibility days at Great Smoky Mountains, TN, as a typical mountain class I area.

In the first tier, SO_2, NO_x, NH_3, VOC (both man-made and biogenic), and PC emissions were reduced by 30%, from their 2018-OTB levels (Table 2), individually and uniformly over the entire domain. During the summer period, SO_2 emission reduction was the most effective control strategy in reducing $PM_{2.5}$ levels because of a large decrease in sulfate concentrations. The SO_2 reduction was also the most beneficial strategy in improving visibility because sulfate is the largest summertime contributor to light extinction in this region. In winter, NH_3 reduction was the most effective strategy because of large reductions in nitrate and ammonium, followed by NO_x and PC reductions. None of the reductions simulated here made visibility so much worse that the estimated value of light extinction exceeded its current (2000–04) value. At some coastal and most mountain sites, NO_x controls increased the sulfate and ammonium levels. This was largest at Cohutta, where ΔB_{ext} from 30% NO_x reduction was $+3.75$ Mm^{-1} but not sufficient to consume the margin of 5.46 Mm^{-1} between the typical baseline and 2018-OTW values of B_{ext}.

The contributions of $PM_{2.5}$ components in the response of B_{ext} to various 30% domainwide emission reductions are shown in Fig. 3 for the Great Smoky Mountains as a typical mountain site. All ammonium contributions were calculated by assuming that sulfates and nitrates are fully neutralized by ammonium. The increase in nitrate as a result of 30% SO_2 reductions amounts to an increase in B_{ext} of 3.34 Mm^{-1} but, after considering the decrease in sulfate and ammonium levels, the net result is a ΔB_{ext} of -33.1 Mm^{-1}. The reason

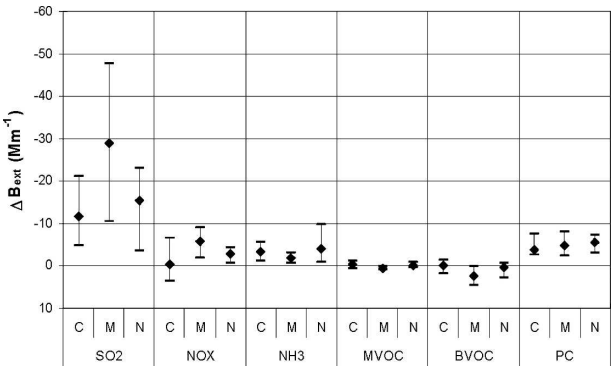

FIG. 4. Response of light extinction to a 30% domainwide decrease in SO_2, NO_x, NH_3, anthropogenic (M)VOC, biogenic (B)VOC, and PC emissions on the 20% worst visibility days at coastal (C), mountain (M), and non-VISTAS (N) class I areas. Diamonds denote the average for each category while bars mark the range.

for the nitrate increase is the availability of more ammonium to form ammonium nitrate (instead of ammonium sulfate) in response to SO_2 reductions. Reduction of NO_x emissions by 30% reduces all $PM_{2.5}$ components and is the second most effective in improving visibility at this site ($\Delta B_{ext} = -6.82$ Mm^{-1}). Ammonia reductions primarily decrease nitrate levels and are less effective ($\Delta B_{ext} = -2.96$ Mm^{-1}) than the same relative amount of PC reductions, which lower OC and EC levels ($\Delta B_{ext} = -4.53$ Mm^{-1}). Note that VOC reductions increase sulfate, nitrate, and ammonium levels and despite decreases in OC levels their net effect is visibility degradation. Reductions in VOC emissions lead to increased ozone and other atmospheric oxidants at rural class I areas that are NO_x limited. Increased atmospheric oxidants lead to increased sulfate and nitrate formation and higher ammonium sulfate and ammonium nitrate levels.

Figure 4 shows the response of light extinction to tier-1 reductions on the 20% worst visibility days. Reducing SO_2 by 30% improves visibility at all sites, most notably at mountain sites. The minimum, maximum, and average B_{ext} decreases are, respectively, 4.80, 21.1, and 11.6 Mm^{-1} for coastal; 10.6, 47.8, and 28.9 Mm^{-1} for mountain; and 3.53, 23.0, and 15.3 Mm^{-1} for non-VISTAS sites. The second largest average B_{ext} decreases result from reducing PC emissions at coastal (3.83 Mm^{-1}) and non-VISTAS sites (5.45 Mm^{-1}) and NO_x emissions at mountain sites (5.85 Mm^{-1}). The NH_3 reduction results in the third largest average B_{ext} decrease at coastal and non-VISTAS sites but it is not very effective at mountain sites. As an exception, the largest decrease in B_{ext} is the result of the 30% NH_3 emission reduction at Brigantine, (9.61 Mm^{-1}), larger than the effect of PC reduction (7.37 Mm^{-1}) and almost three times the effect of SO_2 reduction (3.53 Mm^{-1}). Note that anthropogenic VOC reductions do not result in any noticeable change but biogenic VOC reductions slightly increase B_{ext} in most instances.

An additional question was addressed in this tier. The effects of combined reductions in SO_2, NO_x, and NH_3 emissions were compared with the effects of reducing these emissions individually. It was found that adding individual responses may result in an overestimation of the combined response by about 10%.

In the second tier, SO_2 sources were first differentiated as ground level and elevated. Then, elevated sources in the VISTAS region were differentiated from elevated sources in the rest of the domain. Elevated VISTAS sources were further broken into three categories: elevated but not electric generating unit (non-EGU), coal-fired power plant (CPP), and other power plant (OPP). During the summer period, the daily average SO_2 emissions add up to 21 700 Mg domain wide according to the 2018-OTB scenario. Only 14% of these emissions are from ground-level sources (2960 Mg). Of the elevated-source portion, 48% are from outside the VISTAS region (8905 Mg). In the VISTAS region, 26% of elevated SO_2 emissions are from non-EGU sources (2540 Mg). Approximately 98% of the EGU SO_2 emissions can be categorized as CPP (7165 Mg).

Because most of the worst visibility days occur during summer, with the exception of a few coastal and non-VISTAS class I areas, only the 12–28 July period was simulated with the 30% SO_2 emission reductions in this and the next tier. In Table 1, the number of summertime worst visibility days is shown in parentheses. Note that there are no wintertime 20% worst visibility days at any of the mountain sites and there is only one such day at five coastal and three non-VISTAS sites. However, at four of these sites the number of worst visibility days drops from two (an already small number) to one making the estimated responses considerably less reliable. At sites with worst visibility days in winter, new weights were applied to summer days for the calculation of the annual 20% worst visibility metrics. Because the only worst visibility day at the Everglades was in winter, no response estimates will be reported for this site.

Figure 5 shows ΔB_{ext} resulting from tier-2 reductions at class I areas of the domain. Not counting the total elevated emission category, reduction of CPP emissions of the VISTAS region had the largest impact on visibility at mountain sites: the average decrease in B_{ext} was 16.0 Mm^{-1}. The largest decrease was observed at Mammoth Cave (30.3 Mm^{-1}) and the smallest decreases oc-

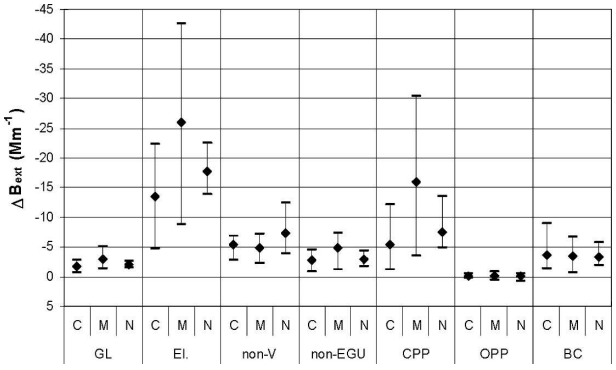

FIG. 5. Response of light extinction to the 30% SO_2 emission reductions from domainwide ground-level (GL) and elevated (El.) sources, elevated sources in non-VISTAS portion of the domain (non-V), elevated but non-EGU sources in 10 VISTAS states, CPP and OPP in VISTAS states, and the response to the 30% decrease in SO_2 and sulfate boundary conditions (BCs) on the 20% worst visibility days at coastal (C), mountain (M), and non-VISTAS (N) class I areas. Diamonds denote the average for each category while bars mark the range. The combined average of non-V, non-EGU, CPP, and OPP is the same as the El. average.

curred at the northern sites (i.e., Shenandoah and Dolly Sods). A number of coal-fired power plants within the VISTAS region are likely responsible for poor visibility at Mammoth Cave. Non-VISTAS and VISTAS non-EGU sources almost tied for the second largest impact at mountain sites. The B_{ext} decreases had a slightly larger average for non-VISTAS (4.89 Mm^{-1}) but a wider range for non-EGU sources. At coastal sites, the average decreases in B_{ext} were almost identical and about 5.35 Mm^{-1} for non-VISTAS elevated and VISTAS CPP SO_2 emission reductions. The range was larger for the CPP category. For non-VISTAS sites the range and average of ΔB_{ext} from VISTAS CPP and non-VISTAS elevated sources were very similar but their individual values differed at each site. In general, the response to 30% ground-level SO_2 reductions was small at each site and the response to OPP reductions was negligible. Also shown in Fig. 5 is the impact of reducing the boundary values of SO_2 and sulfate by 30%. On average, the response of B_{ext} is a decrease of 3.41 Mm^{-1}, a value very similar to the average decrease due to VISTAS non-EGU emission reduction (3.46 Mm^{-1}). This significant contribution can be attributed to sources outside the domain shown in Fig. 1 and indicates how important it is to set the right boundary conditions. Recall that the boundary conditions used (and reduced) here were produced by simulating the same period over continental United States with 36-km grid resolution and 2018-OTB emissions.

In the third tier, CPP and non-EGU emissions of the VISTAS region were further broken down by state as shown in Table 3. The CPP emissions from GA, WV, and AL combined exceed the total of the other seven VISTAS states. Non-EGU SO_2 emissions are more uniformly distributed among the states than the CPP emissions. WV, AL, KY, and VA emit more than the others.

Figure 6a shows the response of light extinction at each class I area to 30% CPP SO_2 emission reductions from the VISTAS states on the 20% worst visibility days. Negative ΔB_{ext}, plotted upward from the origin, indicates a benefit from the reduction. The impact of reductions from each state are color coded and stacked for comparison. The sites are grouped as coastal, mountain, and non-VISTAS and, within each group, ordered from south to north. At Mammoth Cave, for example, the largest contribution to visibility improvement comes from AL ($\Delta B_{ext} = -10.1$ Mm^{-1}) and then from TN ($\Delta B_{ext} = -7.59$ Mm^{-1}) and GA ($\Delta B_{ext} = 6.58$ Mm^{-1}). As a counterintuitive result, reduction of NC CPP emissions by 30% slightly increased sulfate levels and B_{ext} by 0.20 Mm^{-1} at Mammoth Cave. This phenomenon is most likely due to numerical errors rather than any modeled process. The brute-force method can lead to such peculiarities when the level of response to emission perturbations is smaller than the level of numerical errors in the base model. Other states contributed less than 1.5 Mm^{-1} to visibility improvement. The net change in B_{ext} (i.e., the result of adding the contributions of all 10 VISTAS states) was -29.1 Mm^{-1}, the largest decrease at any site. In general, the largest impacts were attributed to the CPP emissions of the nearest states; however, the regional nature of the haze problem cannot be overlooked. For example, Chassahowitzka showed the greatest visibility improvement when WV CPP emissions, a large but very distant source, were reduced. Greater improvements because of CPP SO_2 controls are expected at southern mountain sites when compared with non-VISTAS, coastal,

TABLE 3. CPP and non-EGU elevated SO_2 emissions from the VISTAS states in the 2018-OTB scenario for an average summer day (Mg).

	AL	FL	GA	KY	MS	NC	SC	TN	VA	WV
CPP	1078	576	1373	757	94	315	505	761	408	1298
non-EGU	364	192	224	306	166	201	182	225	301	381

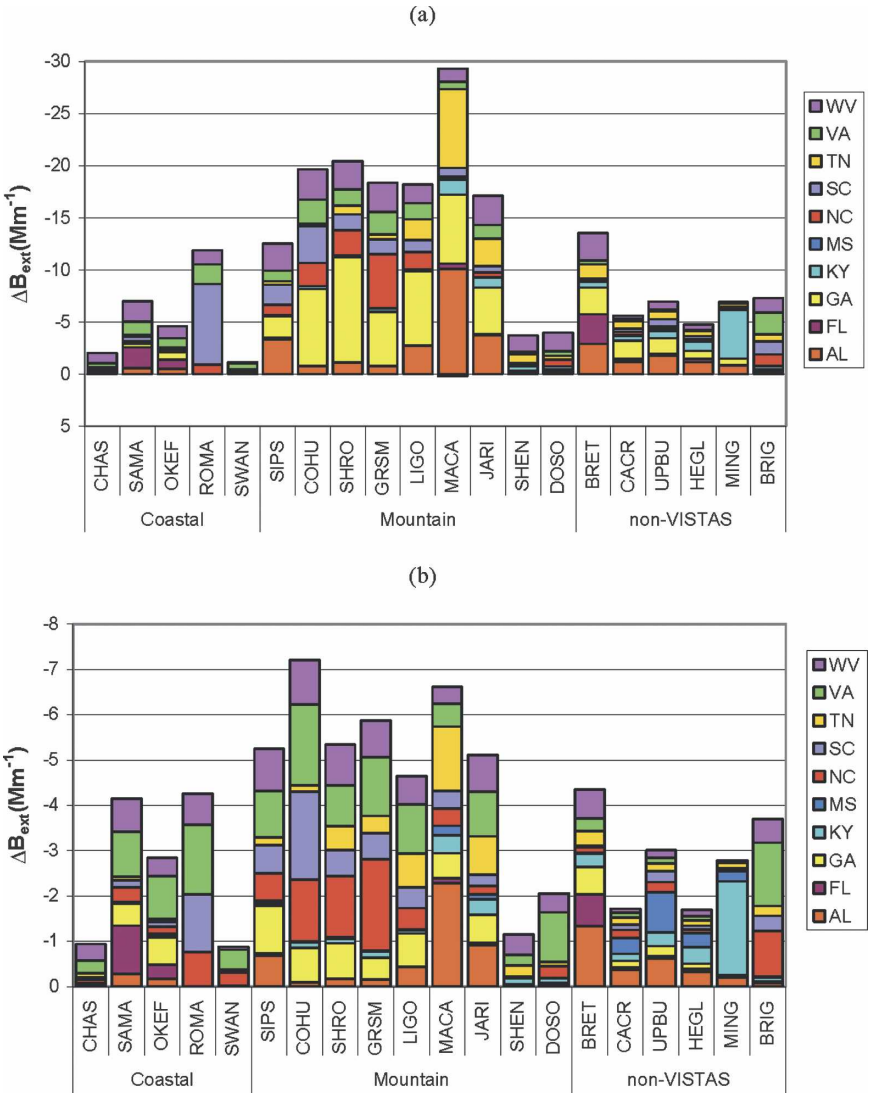

FIG. 6. Response of light extinction to the 30% reduction in SO_2 emissions from (a) CPPs and (b) elevated but non-EGU sources in 10 VISTAS states at coastal, mountain, and non-VISTAS class I areas in the domain.

and northern mountain (Shenandoah and Dolly Sods) sites.

The visibility improvements due to non-EGU SO_2 reductions from each individual VISTAS state show contributions that are more regional in nature (Fig. 6b). At each class I area visibility was affected at a different level by these reductions. The impact of non-EGU SO_2 reductions were, on average, about 36% of the impact of CPP SO_2 reductions, commensurate with the ratio of emissions reduced (35%). Cohutta showed the greatest net benefit with the largest contribution from SC ($\Delta B_{ext} = -1.95$ Mm^{-1}) followed by VA ($\Delta B_{ext} = -1.79$ Mm^{-1}) and NC ($\Delta B_{ext} = -1.37$ Mm^{-1}). GA's contribution ($\Delta B_{ext} = -0.76$ Mm^{-1}) was even less than WV ($\Delta B_{ext} = -0.98$ Mm^{-1}). Once again, southern mountain sites experienced the greatest benefits but the difference from other sites decreased in general.

4. Conclusions

The CMAQ model was used to estimate PM and visibility levels at class I areas of the southeastern United States in the year 2018. The analysis focused on a limited number of simulated days at each class I area in an effort to approximate the annual 20% best/worst visibility metrics. Because only two episodes, one summer and one winter, were simulated not all key meteorological conditions leading to the best/worst visibility

were represented. Therefore, the results of this study should be viewed with some caution.

According to the 2018 on-the-way scenario, which includes the already promulgated clean air interstate rule, only a couple of coastal class I areas in the region are expected to experience visibility degradation on 20% best visibility days. However, SO_2 controls and increasing ammonia emissions may increase nitrate levels at a number of sites. Additional controls may be necessary for reasonable progress toward the goal of achieving natural visibility conditions on the 20% worst visibility days by 2064.

Using 2018 emission projections as the base case, various emission reduction options were simulated using the CMAQ model to evaluate each option in terms of visibility improvement on the 20% worst visibility days and degradation, if any, on the 20% best visibility days. In each option, emissions from a certain source category were reduced by 30% and the visibility response was calculated using model estimated PM concentrations at each class I area. First, domainwide reductions of SO_2, NO_x, NH_3, VOC, and PC emissions were considered. SO_2 reductions showed the largest benefits at the majority of class I areas on the 20% worst visibility days followed by NO_x reductions at mountain sites and PC reductions at other sites. NH_3 reductions were somewhat effective at coastal sites and at class I areas outside the VISTAS region but not at mountain sites, and VOC reductions were ineffective. None of the reductions made visibility worse than current conditions at any class I area.

More detailed analysis of the SO_2 reductions was conducted using the summer episode only. This did not change the number of days considered in the annual 20% worst visibility metric at mountain sites, but reduced it by one at a few other sites making the results less reliable. The 30% reductions in elevated SO_2 emissions were significantly more effective than the 30% ground-level SO_2 reductions. Of these elevated SO_2 sources, coal-fired power plants in the VISTAS region generally had the largest effect on visibility but the impact of elevated sources outside this region were larger for some coastal and non-VISTAS class I areas. Smaller than the impact of these two source categories, the impact of sources outside the domain, simulated by reducing the boundary conditions of sulfur by 30%, were almost as large as the impact of emissions from elevated non–electric generating units (non-EGU) in the VISTAS region.

When the coal-fired power plants of the VISTAS region were broken down by state, visibility at each class I area was affected at a different level by emissions from different states. In general, the largest impacts could be attributed to the closest states; however, the contributions of distant states were often significant. When the non-EGU emissions were broken down by state, the contribution from distant sources became more obvious. This result points to the regional nature of the haze problem and calls for regional control strategies. Quantitative estimates provided here, especially sensitivities to emission reductions from specific states can be used as guidance in the design of emission control strategies. However, the effectiveness of a control strategy should always be checked with simulations.

Acknowledgments. This research was supported by VISTAS under Contract V-2003-12 to the Georgia Institute of Technology.

REFERENCES

Bhave, P. V., S. J. Roselle, F. S. Binkowski, C. G. Nolte, S. Yu, G. L. Gipson, and K. L. Schere, 2004: CMAQ aerosol module development: Recent enhancements and future plans. *Extended Abstracts, Third Annual CMAS Models-3 Users' Conf.,* Chapel Hill, NC, Community Modeling and Analysis System (CMAS) Center. [Available online at http://www.cmascenter.org/conference/2004/archive.html.]

Binkowski, F. S., and S. J. Roselle, 2003: Models-3 Community Multiscale Air Quality (CMAQ) model aerosol component. 1. Model description. *J. Geophys. Res.,* **108,** 4183, doi:10.1029/2001JD001409.

Boylan, J. W., M. T. Odman, J. G. Wilkinson, A. G. Russell, K. G. Doty, W. B. Norris, and R. T. McNider, 2002: Development of a comprehensive multiscale "one atmosphere" modeling system: Application to the southern Appalachian Mountains. *Atmos. Environ.,* **36,** 3721–3734.

——, ——, ——, and ——, 2006: Integrated assessment modeling of atmospheric pollutants in the Southern Appalachian Mountains: Part II—$PM_{2.5}$ and visibility. *J. Air Waste Manage. Assoc.,* **56,** 12–22.

Byun, D. W., and J. K. S. Ching, Eds., 1999: Science algorithms of the EPA Models-3 Community Multiscale Air Quality system. U.S. Environmental Protection Agency, Rep. EPA-600/R-99/030, 768 pp.

Carmichael, G. R., A. Sandu, and F. A. Potra, 1997: Sensitivity analysis for atmospheric chemistry models via automatic differentiation. *Atmos. Environ.,* **31,** 475–489.

Center for Environmental Modeling for Policy Development, 2004: SMOKE version 2.1 user's manual. [Available online at http://cf.unc.edu/cep/empd/products/smoke/version2.1/manual.pdf.]

Chang, S. Y., E. McDonald-Buller, Y. Kimura, G. Yarwood, J. Neece, M. Russell, P. Tanaka, and D. Allen, 2002: Sensitivity of urban ozone formation to chlorine emission estimates. *Atmos. Environ.,* **36,** 4991–5003.

Cohan, D. S., A. Hakami, Y. T. Hu, and A. G. Russell, 2005: Nonlinear response of ozone to emissions: Source apportionment and sensitivity analysis. *Environ. Sci. Technol.,* **39,** 6739–6748.

Douglas, S., B. Hudischewskyj, and Y. Wei, 2006: Characterization of meteorology and its relationships to fine particulate mass and visibility in the VISTAS region. Draft Rep. to VISTAS, Swannanoa, NC, 298 pp.

ENVIRON, 2006: User's guide: Comprehensive Air Quality Model with extensions, version 4.40, ENVIRON, 261 pp. [Available online at http://www.camx.com.]

EPA, 1999: Regional haze regulations: Final rule (Federal Register, 40 CFR Part 51). U.S. Environmental Protection Agency, Washington, DC, 164 pp.

——, 2002: List of 156 mandatory class I federal areas (Federal Register, 40 CFR Part 81). U.S. Environmental Protection Agency, Washington, DC. [Available online at www.epa.gov/oar/vis/class1.html.]

Fast, J. D., and W. E. Heilman, 2005: Simulated sensitivity of seasonal ozone exposure in the Great Lakes region to changes in anthropogenic emissions in the presence of interannual variability. *Atmos. Environ.,* **39,** 5291–5306.

Grell, G. A., J. Dudhia, and D. R. Stauffer, 1994: A description of the fifth-generation Penn State/NCAR Mesoscale Model (MM5). NCAR/TN-398+STR, NCAR, 122 pp.

Hakami, A., M. T. Odman, and A. G. Russell, 2003: High-order, direct sensitivity analysis of multidimensional air quality models. *Environ. Sci. Technol.,* **37,** 2442–2452.

——, ——, and ——, 2004: Nonlinearity in atmospheric response: A direct sensitivity analysis approach. *J. Geophys. Res.,* **109,** D15303, doi:10.1029/2003JD004502.

Harley, R. A., A. G. Russell, G. J. McRae, G. R. Cass, and J. H. Seinfeld, 1993: Photochemical modeling of the Southern California Air Quality Study. *Environ. Sci. Technol.,* **27,** 378–388.

Hwang, D., D. W. Byun, and M. T. Odman, 1997: An automatic differentiation technique for sensitivity analysis of numerical advection schemes in air quality models. *Atmos. Environ.,* **31,** 879–888.

Interagency Monitoring of Protected Visual Environments, 2000: Spatial and seasonal patterns and temporal variability of haze and its constituents in the United States, Rep. III, 384 pp.

Jiang, G. F., and J. D. Fast, 2004: Modeling the effects of VOC and NOX emission sources on ozone formation in Houston during the TexAQS 2000 field campaign. *Atmos. Environ.,* **38,** 5071–5085.

Lin, C. J., T. C. Ho, H. W. Chu, H. Yang, S. Chandru, N. Krishnarajanagar, P. Chiou, and J. R. Hopper, 2005: Sensitivity analysis of ground-level ozone concentration to emission changes in two urban regions of southeast Texas. *J. Environ. Manage.,* **75,** 315–323.

Mallet, V., and B. Sportisse, 2005: A comprehensive study of ozone sensitivity with respect to emissions over Europe with a chemistry-transport model. *J. Geophys. Res.,* **110,** D22302, doi:10.1029/2005JD006234.

Marr, L. C., and R. A. Harley, 2002: Modeling the effect of weekday-weekend differences in motor vehicle emissions on photochemical air pollution in central California. *Environ. Sci. Technol.,* **36,** 4099–4106.

Menut, L., R. Vautard, M. Beekmann, and C. Honore, 2000: Sensitivity of photochemical pollution using the adjoint of a simplified chemistry-transport model. *J. Geophys. Res.,* **105,** 15 379–15 402.

Morris, R. E., and Coauthors, 2004: Model performance evaluation and model sensitivity tests for three Phase I episodes. ENVIRON to VISTAS, 112 pp. [Available online at http://pah.cert.ucr.edu/vistas/reports/Final_Phase1.]

——, D. E. McNally, T. W. Tesche, G. Tonnesen, J. W. Boylan, and P. Brewer, 2005: Preliminary evaluation of the Community Multiscale Air Quality Model for 2002 over the Southeastern United States. *J. Air Waste Manage. Assoc.,* **55,** 1694–1708.

Napelenok, S. L., D. S. Cohan, Y. Hu, and A. G. Russell, 2006: Decoupled direct 3D sensitivity analysis for particulate matter (DDM-3D/PM). *Atmos. Environ.,* **40,** 6112–6121.

Oanh, N. T. K., and B. N. Zhang, 2004: Photochemical smog modeling for assessment of potential impacts of different management strategies on air quality of the Bangkok Metropolitan Region, Thailand. *J. Air Waste Manage. Assoc.,* **54,** 1321–1338.

Odman, M. T., and Coauthors, 2002: Integrated modeling for air quality assessment: The Southern Appalachian Mountains Initiative project. *J. Phys. IV France,* **12,** 211–234.

——, A. G. Russell, and J. W. Boylan, 2004: Estimates of PM2.5 levels in the southeastern United States for the year 2010: What else can be done? *Fuel Process. Technol.,* **85,** 631–639.

Olerud, D., and A. Sims, 2003: MM5 sensitivity modeling in support of VISTAS. Draft Rep. for VISTAS, 112 pp. [Available online at http://www.baronams.com/projects/VISTAS/reports/VISTAS_TASK2e_draft.pdf.]

Pai, P., K. Vijayaraghavan, and C. Seigneur, 2000: Particulate matter modeling in the Los Angeles basin using SAQM-AERO. *J. Air Waste Manage. Assoc.,* **50,** 32–42.

Pison, I., and L. Menut, 2004: Quantification of the impact of aircraft traffic emissions on tropospheric ozone over Paris area. *Atmos. Environ.,* **38,** 971–983.

System Applications International, Inc., 1999: User's Guide to the Variable-Grid Urban Airshed Model (UAM-V). System Applications International, Inc., San Rafael, CA, 415/507-7100, 177 pp. [Available online at http://uamv.saintl.com/documents/uam-v_1.31_user's_guide.pdf.]

Schmidt, H., and D. Martin, 2003: Adjoint sensitivity of episodic ozone in the Paris area to emissions on the continental scale. *J. Geophys. Res.,* **108,** 8561, doi:10.1029/2001JD001583.

Stein, A. F., and D. Lamb, 2002: Chemical indicators of sulfate sensitivity to nitrogen oxides and volatile organic compounds. *J. Geophys. Res.,* **107,** 4449, doi:10.1029/2001JD001088.

Tesche, T. W., R. Morris, G. Tonnesen, D. McNally, J. Boylan, and P. Brewer, 2006: CMAQ/CAMx annual 2002 performance evaluation over the eastern U.S. *Atmos. Environ.,* **40,** 4906–4919.

Vautard, R., M. Beekmann, J. Roux, and D. Gombert, 2001: Validation of a hybrid forecasting system for the ozone concentration over the Paris area. *Atmos. Environ.,* **35,** 2449–2461.

Yang, Y. J., J. G. Wilkinson, and A. G. Russell, 1997: Fast, direct sensitivity analysis of multidimensional photochemical models. *Environ. Sci. Technol.,* **31,** 2859–2868.